Misspecified Cramér-Rao Bound of RIS-Aided Localization Under Geometry Mismatch

Citation for the original published paper (version of record):
Zheng, P., Chen, H., Ballal, T. et al (2023). Misspecified Cramér-Rao Bound of RIS-Aided Localization Under Geometry Mismatch. ICASSP, IEEE International Conference on Acoustics, Speech and Signal Processing - Proceedings, 2023-June.
http://dx.doi.org/10.1109/ICASSP49357.2023.10096904

MISSPECIFIED CRAMÉR-RAO BOUND OF RIS-AIDED LOCALIZATION UNDER GEOMETRY MISMATCH

Pinjun Zheng[⋆]*, Hui Chen*[†]*, Tarig Ballal*[⋆]*, Henk Wymeersch*[†]*, Tareq Y. Al-Naffouri*[⋆]

[⋆]King Abdullah University of Science and Technology, Thuwal, KSA
[†]Chalmers University of Technology, Gothenburg, Sweden

ABSTRACT

In 5G/6G wireless systems, reconfigurable intelligent surfaces (RIS) can play a role as a passive anchor to enable and enhance localization in various scenarios. However, most existing RIS-aided localization works assume that the geometry of the RIS is perfectly known, which is not realistic in practice due to calibration errors. In this work, we derive the misspecified Cramér-Rao bound (MCRB) for a single-input-single-output RIS-aided localization system with RIS geometry mismatch. Specifically, unlike most existing works that use numerical methods, we propose a closed-form solution to the pseudo-true parameter determination problem for MCRB analysis. Simulation results demonstrate the validity of the derived pseudo-true parameters and MCRB, and show that the RIS geometry mismatch causes performance saturation in the high signal-to-noise ratio regions.

***Index Terms*—** Localization, RIS, 5G/6G, geometry mismatch, calibration error, MCRB

1. INTRODUCTION

Reconfigurable intelligent surface (RIS)-aided localization has been extensively studied recently [1, 2, 3]. One of the merits is that RIS enables localization in extreme scenarios. For example, a single-input-single-output (SISO) system consisting of a base station (BS) and a user equipment (UE) can perform communication, but achieving localization is impossible. With the introduction of the RIS channel and the corresponding delay and angle-of-departure (AOD) measurements, however, joint UE localization and synchronization can be completed [4]. RIS is also beneficial in other scenarios such as wireless fingerprinting localization [5], signal strength-based localization [6], localization under mobility [7], user tracking [8], terahertz band localization [9], etc.

Unfortunately, almost all the mentioned systems assume that the RIS position and orientation are perfectly known. However, the geometry mismatch of the RIS is likely to be introduced in reality due to calibration errors. These calibration errors propagate to the estimated channel parameters and cause the model mismatch in the position estimation process. For the mismatched model, the misspecified Cramér-Rao bound (MCRB) is a tool to quantify the impact of the RIS calibration error [10]. When using MCRB, the assumed channel model is different from the true model, and a misspecified performance bound can be derived with the model mismatch considered. The MCRB analysis for radio localization under hardware impairment [11] and channel model mismatch [12] have been reported in previous works. In the MCRB derivation, one of the most essential steps is determining the pseudo-true parameters [10], which is to find a solution that minimizes the Kullback–Leibler divergence (KLD) between the true and mismatched statistical models and is usually accomplished using numerical methods [11, 12]. In this work, we aim to derive the MCRB to evaluate the impact of RIS geometry mismatch on RIS-assisted localization. The main contribution of this work is that we derive a *closed-form* solution to the pseudo-true parameter determination problem. The corresponding geometrical interpretation is also given. The simulation code of this paper is available at `https://github.com/ZPinjun/RISgeoMCRB2023ICASSP`.

2. SYSTEM MODEL

2.1. Geometrical Relations

We consider a downlink SISO wireless system with a BS, a UE, and a RIS, as shown in Fig. 1. We indicate the position of the BS and the UE by $\mathbf{p}_{\mathrm{b}} \in \mathbb{R}^3$ and $\mathbf{p} \in \mathbb{R}^3$. The position and orientation of the RIS are denoted as $\mathbf{p}_{\mathrm{r}} \in \mathbb{R}^3$ and $\mathbf{R}_{\mathrm{r}} \in \mathrm{SO(3)}$ [13], respectively. The entries of $\mathbf{p}_{\mathrm{b}}$, $\mathbf{p}_{\mathrm{r}}$, and $\mathbf{R}_{\mathrm{r}}$ are assumed to be known. Besides, we assume an unknown clock bias $\Delta \in \mathbb{R}$ exists between the UE and the BS [14, 15].

In the RIS's local coordinate system (LCS), the angle-of-arrival (AOA) from the BS consists of an azimuth angle θ_{az} and an elevation angle θ_{el}, while the AOD towards the UE consists of an azimuth angle ϕ_{az} and an elevation angle ϕ_{el}. For compactness, we define $\boldsymbol{\theta} = [\theta_{\mathrm{az}}, \theta_{\mathrm{el}}]^{\mathsf{T}}$ and $\boldsymbol{\phi} = [\phi_{\mathrm{az}}, \phi_{\mathrm{el}}]^{\mathsf{T}}$. Since we assume the geometry of the BS and the

This work is supported by KAUST Office of Sponsored Research (OSR) under Award No. ORA-CRG2021-4695, and by the European Commission through the EU H2020 RISE-6G project under grant 101017011.

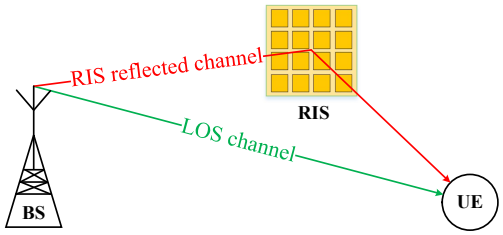

Fig. 1. Illustration of a RIS-aided localization system.

RIS to be known in the ideal model, we focus on the AOD towards the UE with an unknown position, which is given by

$$\phi_{\text{az}} = \arctan 2\left([\mathbf{R}_{\text{r}}^{\mathsf{T}}(\mathbf{p}-\mathbf{p}_{\text{r}})]_2, [\mathbf{R}_{\text{r}}^{\mathsf{T}}(\mathbf{p}-\mathbf{p}_{\text{r}})]_1\right), \quad (1)$$

$$\phi_{\text{el}} = \arcsin\left([\mathbf{R}_{\text{r}}^{\mathsf{T}}(\mathbf{p}-\mathbf{p}_{\text{r}})]_3/\|\mathbf{p}-\mathbf{p}_{\text{r}}\|\right), \quad (2)$$

where $[\cdot]_i$ represents the i-th element of a vector. The delays over the BS-UE line-of-sight (LOS) and the BS-RIS-UE none-line-of-sight (NLOS) paths are given by

$$\tau_{\text{b}} = \|\mathbf{p}_{\text{b}}-\mathbf{p}\|/c + \Delta, \quad (3)$$

$$\tau_{\text{r}} = \|\mathbf{p}_{\text{b}}-\mathbf{p}_{\text{r}}\|/c + \|\mathbf{p}_{\text{r}}-\mathbf{p}\|/c + \Delta, \quad (4)$$

where c is the speed of light.

2.2. Channel Model

We consider the transmission of L orthogonal frequency-division multiplexing (OFDM) pilot symbols with K subcarriers. The frequency of the k-th subcarrier is denoted as $f_k = f_c + \frac{(2k-1-K)}{2}\Delta_f, k = 1,\ldots,K$, where $\Delta_f = B/K$ is the subcarrier spacing, f_c is the carrier frequency, and B is the bandwidth. The received baseband signal in the OFDM block with index ℓ is given by [14]

$$\mathbf{y}_\ell = \underbrace{\overbrace{g_{\text{b}}\mathbf{d}(\tau_{\text{b}})\odot\mathbf{x}}^{\text{LOS channel}} + \overbrace{g_{\text{r}}\mathbf{b}(\boldsymbol{\phi})^{\mathsf{T}}\boldsymbol{\gamma}_\ell(\mathbf{d}(\tau_{\text{r}})\odot\mathbf{x})}^{\text{RIS reflected channel}}}_{\boldsymbol{\mu}_\ell} + \mathbf{n}, \quad (5)$$

where g_{b} and g_{r} indicate the complex channel gain for the LOS path and the RIS reflected path, $\boldsymbol{\gamma}_\ell$ is the RIS phase profile, $\mathbf{x}$ is the transmitted signal, $\mathbf{n} \sim \mathcal{CN}(\mathbf{0}, \sigma^2\mathbf{I}_K)$ is a complex additive white Gaussian noise (AWGN) vector, and $\boldsymbol{\mu}_\ell$ is the noise-free version of the received signal. The vector $\mathbf{d}(\tau)$ is the delay steering vector defined as

$$\mathbf{d}(\tau) = [1, e^{-j2\pi\Delta_f\tau}, \ldots, e^{-j2\pi(K-1)\Delta_f\tau}]^{\mathsf{T}}. \quad (6)$$

Moreover, $\mathbf{b}(\boldsymbol{\phi}) \triangleq \mathbf{a}(\boldsymbol{\theta}) \odot \mathbf{a}(\boldsymbol{\phi})$, where $\mathbf{a}(\boldsymbol{\theta})$ and $\mathbf{a}(\boldsymbol{\phi})$ are respectively the array response vectors for the AOA and AOD of the RIS. Under the narrowband far-field model, the array response vector of the RIS can be described as $[\mathbf{a}(\boldsymbol{\alpha})]_i = e^{j\frac{2\pi f_c}{c}\mathbf{t}(\boldsymbol{\alpha})^{\mathsf{T}}\mathbf{p}_i}$, where $\mathbf{p}_i$ is the position of the i-th RIS element given in its LCS, and $\mathbf{t}(\boldsymbol{\alpha})$ is the direction vector defined as

$$\mathbf{t}(\boldsymbol{\alpha}) \triangleq \left[\cos(\alpha_{\text{az}})\cos(\alpha_{\text{el}}),\ \sin(\alpha_{\text{az}})\cos(\alpha_{\text{el}}),\ \sin(\alpha_{\text{el}})\right]^{\mathsf{T}}.$$

2.3. Geometry Mismatch

Taking the BS's position as a reference, we can focus on the calibration errors in $\mathbf{p}_{\text{r}}$ and $\mathbf{R}_{\text{r}}$. Thus, the accessible prior geometry information of the RIS can be modeled as

$$\tilde{\mathbf{p}}_{\text{r}} = \mathbf{p}_{\text{r}} + \mathbf{u}, \qquad \tilde{\mathbf{R}}_{\text{r}} = \mathbf{R}_{\text{p}}(\mathbf{v})\mathbf{R}_{\text{r}}, \quad (7)$$

where $\mathbf{u}$ and $\mathbf{v}$ are the calibration errors that cause the mismatch in the model. Here, $\mathbf{R}_{\text{p}}(\mathbf{v}) = \mathbf{R}_z(v_3)\mathbf{R}_y(v_2)\mathbf{R}_x(v_1)$, where $\mathbf{R}_x(v_1)$ denotes a rotation of v_1 degree around the X-axis, and likewise for $\mathbf{R}_y(v_2)$ and $\mathbf{R}_z(v_3)$.

3. LOCALIZATION LOWER BOUND

3.1. Misspecified Cramér-Rao Bound

Suppose a two-stage localization framework is employed [16, 17], that consists of a channel parameter estimation process followed by a UE location estimation from the obtained channel parameters. For the channel parameter estimation stage, we estimate the following channel parameters from the received signal $\mathbf{y}_\ell, \ell = 1,\ldots,L$ given in (5):

$$\boldsymbol{\eta}_{\text{ch}} \triangleq [\phi_{\text{az}}, \phi_{\text{el}}, \tau_{\text{b}}, \tau_{\text{r}}, \Re(g_{\text{b}}), \Im(g_{\text{b}}), \Re(g_{\text{r}}), \Im(g_{\text{r}})]^{\mathsf{T}}, \quad (8)$$

where $\Re(\cdot)$ / $\Im(\cdot)$ denote the operations of taking the real / imaginary part. The Fisher information matrix (FIM) of $\boldsymbol{\eta}_{\text{ch}}$ can be calculated by the Slepian-Bangs formula [18, Sec. 3.4]

$$\mathbf{J}(\boldsymbol{\eta}_{\text{ch}}) = \frac{2}{\sigma^2}\sum_{\ell=1}^{L}\Re\left(\left(\frac{\partial\boldsymbol{\mu}_\ell}{\partial\boldsymbol{\eta}_{\text{ch}}}\right)^{\mathsf{H}}\frac{\partial\boldsymbol{\mu}_\ell}{\partial\boldsymbol{\eta}_{\text{ch}}}\right). \quad (9)$$

By removing the nuisance parameters related to g_{b} and g_{r}, we further define $\boldsymbol{\eta} \triangleq [\phi_{\text{az}}, \phi_{\text{el}}, \tau_{\text{b}}, \tau_{\text{r}}]^{\mathsf{T}}$ used for position and orientation estimation. We can compute the FIM for $\boldsymbol{\eta}$ using Schur's complement: we partition $\mathbf{J}(\boldsymbol{\eta}_{\text{ch}}) = [\mathbf{X}, \mathbf{Y}; \mathbf{Y}^{\mathsf{T}}, \mathbf{Z}]$, where $\mathbf{X} \in \mathbb{R}^{4\times4}$ so that $\mathbf{J}(\boldsymbol{\eta}) = \mathbf{X} - \mathbf{Y}\mathbf{Z}^{-1}\mathbf{Y}^{\mathsf{T}}$.

For the UE location estimation, we define a parameter vector in the location domain as $\mathbf{r} \triangleq [\mathbf{p}^{\mathsf{T}}, \Delta]^{\mathsf{T}} \in \mathbb{R}^4$. The objective here is to estimate $\mathbf{r}$ from the estimated $\hat{\boldsymbol{\eta}}$, where the RIS geometry mismatch occurs. We express $\boldsymbol{\eta}$ as a function of $\mathbf{r}$, i.e., $\boldsymbol{\eta} = \mathbf{g}(\mathbf{r}|\mathbf{p}_{\text{b}}, \mathbf{p}_{\text{r}}, \mathbf{R}_{\text{r}})$, a relationship that is defined by (1)-(4). Thus, the distribution of the estimated $\hat{\boldsymbol{\eta}}$ can be obtained as $\hat{\boldsymbol{\eta}} \sim \mathcal{N}(\mathbf{g}(\mathbf{r}|\mathbf{p}_{\text{b}}, \mathbf{p}_{\text{r}}, \mathbf{R}_{\text{r}}), \boldsymbol{\Sigma})$, where $\boldsymbol{\Sigma} = \mathbf{J}^{-1}(\boldsymbol{\eta})$ if an *efficient* channel estimator is applied in the first stage. To estimate $\mathbf{r}$, however, we adopt the mismatched model by using $\hat{\boldsymbol{\eta}} \sim \mathcal{N}\left(\mathbf{g}(\mathbf{r}|\mathbf{p}_{\text{b}}, \tilde{\mathbf{p}}_{\text{r}}, \tilde{\mathbf{R}}_{\text{r}}), \boldsymbol{\Sigma}\right)$ to obtain an estimate $\hat{\mathbf{r}}$ from $\hat{\boldsymbol{\eta}}$. Then, we have the true likelihood function (f_{T}) and the mismatched likelihood function (f_{M}) as

$$\ln f_{\text{T}} = -\frac{1}{2}(\hat{\boldsymbol{\eta}} - \mathbf{g}(\mathbf{r}|\mathbf{p}_{\text{r}}, \mathbf{R}_{\text{r}}))^{\mathsf{T}}\boldsymbol{\Sigma}^{-1}(\hat{\boldsymbol{\eta}} - \mathbf{g}(\mathbf{r}|\mathbf{p}_{\text{r}}, \mathbf{R}_{\text{r}})),$$

$$\ln f_{\text{M}} = -\frac{1}{2}(\hat{\boldsymbol{\eta}} - \mathbf{g}(\mathbf{r}|\tilde{\mathbf{p}}_{\text{r}}, \tilde{\mathbf{R}}_{\text{r}}))^{\mathsf{T}}\boldsymbol{\Sigma}^{-1}(\hat{\boldsymbol{\eta}} - \mathbf{g}(\mathbf{r}|\tilde{\mathbf{p}}_{\text{r}}, \tilde{\mathbf{R}}_{\text{r}})).$$

Note that we omit the constant term and the parameter $\mathbf{p}_{\text{b}}$ as they do not affect the estimation.

Now, the lower bound matrix of the estimation mean squared error (MSE) based on f_{M} can be obtained as [12]

$$\mathrm{LBM}(\hat{\mathbf{r}},\bar{\mathbf{r}}) = \underbrace{\mathbf{A}_{\mathbf{r}_0}^{-1}\mathbf{B}_{\mathbf{r}_0}\mathbf{A}_{\mathbf{r}_0}^{-1}}_{\mathrm{MCRB}(\mathbf{r}_0)} + \underbrace{(\bar{\mathbf{r}}-\mathbf{r}_0)(\bar{\mathbf{r}}-\mathbf{r}_0)^{\mathsf{T}}}_{\mathrm{Bias}(\mathbf{r}_0)}, \quad (10)$$

where $\bar{\mathbf{r}}$ is the true parameter vector, $\mathbf{r}_0$ is the pseudo-true parameter vector that minimizes the KLD between f_{T} and f_{M}. $\mathbf{A}_{\mathbf{r}_0}$ and $\mathbf{B}_{\mathbf{r}_0}$ are two generalizations of the FIMs as [10]

$$\mathbf{r}_0 = \arg\min_{\mathbf{r}} D(f_{\mathrm{T}}(\hat{\boldsymbol{\eta}}|\bar{\mathbf{r}})\|f_{\mathrm{M}}(\hat{\boldsymbol{\eta}}|\mathbf{r})), \quad (11)$$

$$\begin{aligned}[\mathbf{A}_{\mathbf{r}_0}]_{i,j} &= \mathbb{E}_{f_{\mathrm{T}}}\left\{\frac{\partial^2}{\partial r_i \partial r_j}\ln f_{\mathrm{M}}(\hat{\boldsymbol{\eta}}|\mathbf{r})\Big|_{\mathbf{r}=\mathbf{r}_0}\right\}, \quad (12)\\ &= \left(\frac{\partial^2 \mathbf{g}(\mathbf{r}|\tilde{\mathbf{p}}_{\mathrm{r}},\tilde{\mathbf{o}}_{\mathrm{r}})}{\partial r_i \partial r_j}\right)^{\mathsf{T}}\boldsymbol{\Sigma}^{-1}(\boldsymbol{\eta}-\mathbf{g}(\mathbf{r}|\tilde{\mathbf{p}}_{\mathrm{r}},\tilde{\mathbf{o}}_{\mathrm{r}}))\Big|_{\mathbf{r}=\mathbf{r}_0}\\ &\quad - \left(\frac{\partial \mathbf{g}(\mathbf{r}|\tilde{\mathbf{p}}_{\mathrm{r}},\tilde{\mathbf{o}}_{\mathrm{r}})}{\partial r_i}\right)^{\mathsf{T}}\boldsymbol{\Sigma}^{-1}\frac{\partial \mathbf{g}(\mathbf{r}|\tilde{\mathbf{p}}_{\mathrm{r}},\tilde{\mathbf{o}}_{\mathrm{r}})}{\partial r_j}\Big|_{\mathbf{r}=\mathbf{r}_0},\end{aligned}$$

$$\begin{aligned}\mathbf{B}_{\mathbf{r}_0} &= \mathbb{E}_{f_{\mathrm{T}}}\left\{\frac{\partial \ln f_{\mathrm{M}}(\hat{\boldsymbol{\eta}}|\mathbf{r})}{\partial \mathbf{r}}\Big|_{\mathbf{r}=\mathbf{r}_0}\cdot\left(\frac{\partial \ln f_{\mathrm{M}}(\hat{\boldsymbol{\eta}}|\mathbf{r})}{\partial \mathbf{r}}\Big|_{\mathbf{r}=\mathbf{r}_0}\right)^{\mathsf{T}}\right\},\\ &= \left(\frac{\partial \mathbf{g}(\mathbf{r}|\tilde{\mathbf{p}}_{\mathrm{r}},\tilde{\mathbf{o}}_{\mathrm{r}})}{\partial \mathbf{r}}\right)^{\mathsf{T}}\boldsymbol{\Sigma}^{-1}\tilde{\boldsymbol{\Sigma}}(\mathbf{r})\boldsymbol{\Sigma}^{-1}\frac{\partial \mathbf{g}(\mathbf{r}|\tilde{\mathbf{p}}_{\mathrm{r}},\tilde{\mathbf{o}}_{\mathrm{r}})}{\partial \mathbf{r}}\Big|_{\mathbf{r}=\mathbf{r}_0},\end{aligned}$$

where $D(\cdot\|\cdot)$ denotes the KLD and $\tilde{\boldsymbol{\Sigma}}(\mathbf{r}) = \boldsymbol{\Sigma} + (\boldsymbol{\eta} - \mathbf{g}(\mathbf{r}|\tilde{\mathbf{p}}_{\mathrm{r}},\tilde{\mathbf{o}}_{\mathrm{r}}))(\boldsymbol{\eta} - \mathbf{g}(\mathbf{r}|\tilde{\mathbf{p}}_{\mathrm{r}},\tilde{\mathbf{o}}_{\mathrm{r}}))^{\mathsf{T}}$. Therefore, the remaining problem is solving (11) to obtain the pseudo-true parameter $\mathbf{r}_0$. As mentioned, most previous works on localization mismatch analysis solve (11) using numerical methods, e.g., gradient descent, which is time-consuming and offers no guarantees to obtain the global minimum. The next subsection presents a closed-form solution to the pseudo-true parameter estimation problem with the global minimum guarantee.

3.2. The Closed-form Pseudo-true Parameter Vector

In this subsection, we derive a closed-form solution for (11). According to the definition of KLD, we have

$$\begin{aligned}&D(f_{\mathrm{T}}(\hat{\boldsymbol{\eta}}|\bar{\mathbf{r}})\|f_{\mathrm{M}}(\hat{\boldsymbol{\eta}}|\mathbf{r})) = \mathbb{E}_{f_{\mathrm{T}}}\left\{\ln f_{\mathrm{T}}(\hat{\boldsymbol{\eta}}|\bar{\mathbf{r}}) - \ln f_{\mathrm{M}}(\hat{\boldsymbol{\eta}}|\mathbf{r})\right\},\\ &= -\frac{1}{2}\mathbb{E}_{f_{\mathrm{T}}}\left\{(\hat{\boldsymbol{\eta}}-\mathbf{g}(\bar{\mathbf{r}}|\mathbf{p}_{\mathrm{r}},\mathbf{R}_{\mathrm{r}}))^{\mathsf{T}}\boldsymbol{\Sigma}^{-1}(\hat{\boldsymbol{\eta}}-\mathbf{g}(\bar{\mathbf{r}}|\mathbf{p}_{\mathrm{r}},\mathbf{R}_{\mathrm{r}}))\right\}\\ &\quad + \frac{1}{2}\mathbb{E}_{f_{\mathrm{T}}}\left\{(\hat{\boldsymbol{\eta}}-\mathbf{g}(\mathbf{r}|\tilde{\mathbf{p}}_{\mathrm{r}},\tilde{\mathbf{R}}_{\mathrm{r}}))^{\mathsf{T}}\boldsymbol{\Sigma}^{-1}(\hat{\boldsymbol{\eta}}-\mathbf{g}(\mathbf{r}|\tilde{\mathbf{p}}_{\mathrm{r}},\tilde{\mathbf{R}}_{\mathrm{r}}))\right\},\\ &\overset{(a)}{=} \frac{1}{2}\mathbf{h}(\mathbf{r})^{\mathsf{T}}\boldsymbol{\Sigma}^{-1}\mathbf{h}(\mathbf{r}), \quad (13)\end{aligned}$$

where $\mathbf{h}(\mathbf{r}) \triangleq \mathbf{g}(\bar{\mathbf{r}}|\mathbf{p}_{\mathrm{r}},\mathbf{R}_{\mathrm{r}}) - \mathbf{g}(\mathbf{r}|\tilde{\mathbf{p}}_{\mathrm{r}},\tilde{\mathbf{R}}_{\mathrm{r}})$ and step (a) can be obtained by using [19, Eq. 380]. Since $\boldsymbol{\Sigma}$ is a covariance matrix, then $\boldsymbol{\Sigma}^{-1}$ is positive definite. Hence, the quadratic form (13) always satisfies

$$D(f_{\mathrm{T}}(\hat{\boldsymbol{\eta}}|\bar{\mathbf{r}})\|f_{\mathrm{M}}(\hat{\boldsymbol{\eta}}|\mathbf{r})) = \frac{1}{2}\mathbf{h}(\mathbf{r})^{\mathsf{T}}\boldsymbol{\Sigma}^{-1}\mathbf{h}(\mathbf{r}) \geqslant 0, \quad (14)$$

where the equality holds if and only if $\mathbf{h}(\mathbf{r}) = \mathbf{0}$. The inequality in (14) implies that if there exists a vector $\mathbf{r}_0$ that satisfies $\mathbf{h}(\mathbf{r}_0) = \mathbf{0}$, then it must be the global minimum of (11). The following steps aim to find such a vector $\mathbf{r}_0$, which is possible in the considered problem since the number of unknowns ($\mathbf{r} \in \mathbb{R}^4$) equals the number of observations ($\mathbf{h}(\mathbf{r}) \in \mathbb{R}^4$).

Let $\mathbf{r}_0 = [\mathbf{p}_0^{\mathsf{T}}, \Delta_0]^{\mathsf{T}}$ be the pseudo-true parameters and $[\bar{\mathbf{p}}^{\mathsf{T}}, \bar{\Delta}]^{\mathsf{T}} = \bar{\mathbf{r}}$, then $\mathbf{h}(\mathbf{r}_0) = \mathbf{0}$ can be rewritten based on (1)–(4) as

$$\|\mathbf{p}_{\mathrm{b}} - \bar{\mathbf{p}}\| + c\bar{\Delta} = \|\mathbf{p}_{\mathrm{b}} - \mathbf{p}_0\| + c\Delta_0, \quad (15)$$

$$\begin{aligned}\|\mathbf{p}_{\mathrm{b}} - \mathbf{p}_{\mathrm{r}}\| + \|\mathbf{p}_{\mathrm{r}} - \bar{\mathbf{p}}\| + c\bar{\Delta} &= \|\mathbf{p}_{\mathrm{b}} - \tilde{\mathbf{p}}_{\mathrm{r}}\|\\ &\quad + \|\tilde{\mathbf{p}}_{\mathrm{r}} - \mathbf{p}_0\| + c\Delta_0, \quad (16)\end{aligned}$$

$$\mathbf{R}_{\mathrm{r}}^{\mathsf{T}}(\bar{\mathbf{p}} - \mathbf{p}_{\mathrm{r}})/\|\bar{\mathbf{p}} - \mathbf{p}_{\mathrm{r}}\| = \tilde{\mathbf{R}}_{\mathrm{r}}^{\mathsf{T}}(\mathbf{p}_0 - \tilde{\mathbf{p}}_{\mathrm{r}})/\|\mathbf{p}_0 - \tilde{\mathbf{p}}_{\mathrm{r}}\|. \quad (17)$$

Combining (15)–(17), we obtain

$$(\alpha + \|\mathbf{p}_0 - \tilde{\mathbf{p}}_{\mathrm{r}}\| - \|\mathbf{p}_0 - \mathbf{p}_{\mathrm{b}}\|)\frac{\mathbf{p}_0 - \tilde{\mathbf{p}}_{\mathrm{r}}}{\|\mathbf{p}_0 - \tilde{\mathbf{p}}_{\mathrm{r}}\|} = \tilde{\mathbf{R}}_{\mathrm{r}}\mathbf{R}_{\mathrm{r}}^{\mathsf{T}}(\bar{\mathbf{p}} - \mathbf{p}_{\mathrm{r}}), \quad (18)$$

where $\alpha = \|\mathbf{p}_{\mathrm{b}} - \tilde{\mathbf{p}}_{\mathrm{r}}\| + \|\mathbf{p}_{\mathrm{b}} - \bar{\mathbf{p}}\| - \|\mathbf{p}_{\mathrm{b}} - \mathbf{p}_{\mathrm{r}}\|$. From (18), it can be inferred that a pseudo-true UE position can be obtained as the intersection of a line s_l and a hyperboloid s_h given by

$$s_l: \quad \mathbf{p} = x\tilde{\mathbf{R}}_{\mathrm{r}}\mathbf{R}_{\mathrm{r}}^{\mathsf{T}}(\bar{\mathbf{p}} - \mathbf{p}_{\mathrm{r}}) + \tilde{\mathbf{p}}_{\mathrm{r}}, \quad (19)$$

$$s_h: \quad \|\mathbf{p} - \tilde{\mathbf{p}}_{\mathrm{r}}\| - \|\mathbf{p} - \mathbf{p}_{\mathrm{b}}\| = \beta, \quad (20)$$

where x is a positive scalar representing the length of the line segment, and $\beta = \|\bar{\mathbf{p}} - \mathbf{p}_{\mathrm{r}}\| - \alpha$. As a result, the pseudo-true UE position can be determined by solving x, which is

$$x_0 = \frac{\beta^2 - \|\tilde{\mathbf{p}}_{\mathrm{r}} - \mathbf{p}_{\mathrm{b}}\|^2}{2[\mathbf{a}^{\mathsf{T}}(\tilde{\mathbf{p}}_{\mathrm{r}} - \mathbf{p}_{\mathrm{b}}) + \beta\|\mathbf{a}\|]}, \quad (21)$$

with $\mathbf{a} = \tilde{\mathbf{R}}_{\mathrm{r}}\mathbf{R}_{\mathrm{r}}^{\mathsf{T}}(\bar{\mathbf{p}} - \mathbf{p}_{\mathrm{r}})$. Then, the pseudo-true UE position ($\mathbf{p}_0$) is obtained by substituting x_0 into (19). An estimate of pseudo-true clock bias Δ_0 can be directly determined from (15) given $\mathbf{p}_0$.

3.3. Mismatched Bound and Estimator

Based on (10), the expected root mean square error (RMSE) of the UE position estimation (under RIS geometry mismatch) can be lower bounded as

$$\sqrt{\mathbb{E}\{\|\mathbf{p} - \hat{\mathbf{p}}\|^2\}} \geq \sqrt{\mathrm{tr}\big([\mathrm{LBM}(\hat{\mathbf{r}},\bar{\mathbf{r}})]_{1:3,1:3}\big)} \triangleq \mathrm{LB}, \quad (22)$$

where $\mathrm{tr}(\cdot)$ returns the trace of a matrix.

To verify the derived MCRB, we formulate a maximum likelihood (ML)-based localization estimator. To simplify the analysis, we assume that an efficient estimator is applied to obtain the channel parameters $\hat{\boldsymbol{\eta}}$. As such, we focus on analyzing the UE position estimation stage where the mismatch impact appears. Hence we have the following misspecified maximum likelihood (MML) estimation:

$$\hat{\mathbf{r}}_{\mathrm{MML}} = \arg\max_{\mathbf{r}} \ \ln f_{\mathrm{M}}(\hat{\boldsymbol{\eta}}_{\mathrm{ch}}|\mathbf{r}), \quad (23)$$

which can be solved using the gradient descent method.

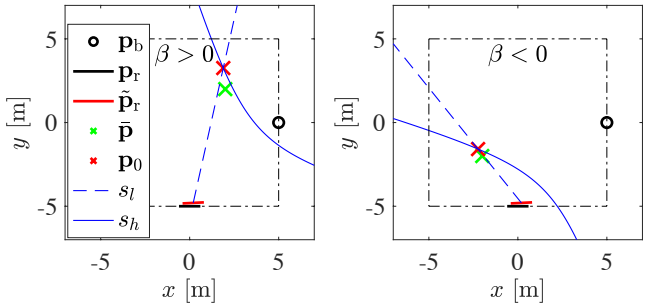

Fig. 2. The geometric relationship between the pseudo-true UE position $\mathbf{p}_0$ and true UE position $\bar{\mathbf{p}}$.

4. SIMULATION RESULTS

4.1. Simulation Setup

We consider a localization system that consists of a BS at $[5, 0, 3]^\mathsf{T}$, a RIS at $[0, -5, 2.5]^\mathsf{T}$ with orientation $\mathbf{o}_\mathrm{r} = [0°, 0°, 90°]$, and a UE with the default location $[-2.5, 2.5, 0]^\mathsf{T}$. The RIS is of size 64×64 elements with half-wavelength spacing. The other parameters are as follows: average transmission power $P = 10\,\mathrm{dBm}$, carrier frequency $f_c = 28\,\mathrm{GHz}$, bandwidth $W = 400\,\mathrm{MHz}$, number of transmissions $L = 32$, number of subcarriers $K = 3000$, noise PSD $N_0 = -173.855\,\mathrm{dBm/Hz}$ and noise figure $N_f = 10\,\mathrm{dB}$.

4.2. Results Analysis

We first present the geometry relationship between the pseudo-true UE position $\mathbf{p}_0$ and the true UE position $\bar{\mathbf{p}}$. We set a fixed RIS position and orientation mismatch error as $\mathbf{u} = 0.2 \times \mathbf{1}\,\mathrm{m}$ and $\mathbf{v} = 3 \times \mathbf{1}\,\mathrm{deg}$, respectively. Fig. 2 shows the projection of the corresponding geometry onto the XOY plane. We can see that the RIS geometry mismatch causes a deviation between the true and pseudo-true UE position, and the pseudo-true UE position $\mathbf{p}_0$ (obtained by solving (11) with a gradient descent method) coincides with the intersection of the line s_l and hyperboloid s_h, which affirms the solution stated in Subsection 3.2. We can also observe that depending on the position of the UE, either $\beta > 0$ or $\beta < 0$ can occur. An example of each case is shown in Fig. 2.

Next, we evaluate the position estimation performance of the estimator (23) and compare it with the theoretical bound LB (22) to validate the derived pseudo-true parameter vector $\mathbf{r}_0$ and the MCRB. Fig. 3 shows the RMSE for the ML estimator [20], LB, bias term, and the mismatch-free position error bound (PEB) versus different transmitted power for a RIS position mismatch ($\mathbf{u} = 0.01 \times \mathbf{1}\,\mathrm{m}$) and orientation mismatch ($\mathbf{v} = 0.5 \times \mathbf{1}\,\mathrm{deg}$) separately. We can observe that at low transmit power (i.e., low signal-to-noise ratio (SNR) given a fixed noise) levels, the LB and the mismatch-free PEB coincide, implying that the RIS geometry mismatch is not the main source of error. At higher signal SNR, however, LB deviates from the mismatch-free PEB and saturates, which reveals the positioning performance is thus more severely affected by the RIS geometry mismatch. The RMSE of the ML estimator closely follows the LB, which demonstrates the validity of our derivation.

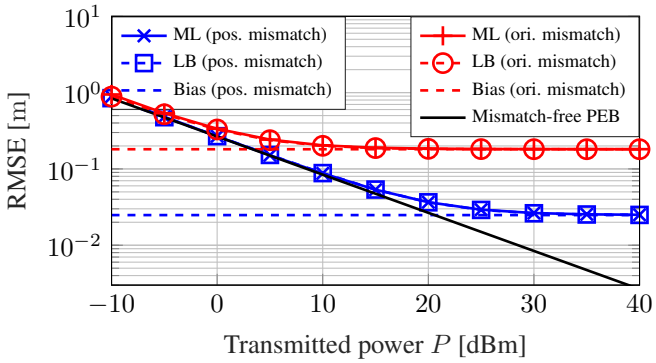

Fig. 3. ML-RMSE, LB, and bias term versus transmitted power (SNR) for RIS position mismatch ($\mathbf{u} = 0.01 \times \mathbf{1}\,\mathrm{m}$) and orientation mismatch ($\mathbf{v} = 0.5 \times \mathbf{1}\,\mathrm{deg}$).

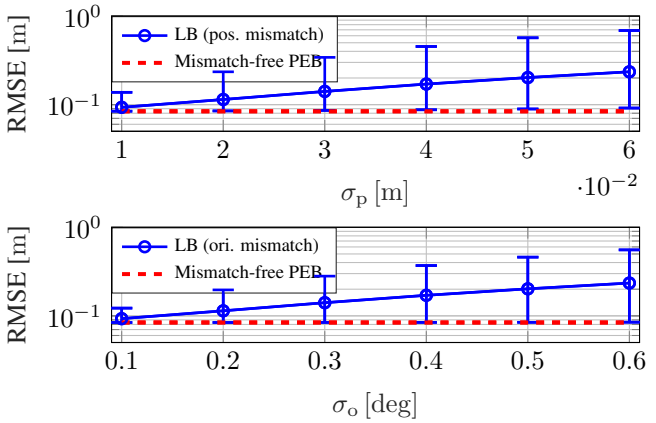

Fig. 4. LB and PEB versus different levels of RIS position mismatch ($\sigma_\mathrm{p} = \{1, 2, 3, 4, 5, 6\} \times 10^{-2}\,\mathrm{m}$) and orientation mismatch ($\sigma_\mathrm{o} = \{1, 2, 3, 4, 5, 6\} \times 10^{-1}\,\mathrm{deg}$).

Finally, in Fig.4, we evaluate the localization performance as a function of the standard deviation of the mismatch errors. We assume $\mathbf{u} \sim \mathcal{N}(\mathbf{0}, \sigma_\mathrm{p}^2 \mathbf{I}_3)$, $\mathbf{v} \sim \mathcal{N}(\mathbf{0}, \sigma_\mathrm{o}^2 \mathbf{I}_3)$, and generate 100 statistical realizations of the mismatch for each standard deviation value and collect the minimum, maximum, and mean values of the LBs. It can be seen that, for both position and orientation mismatches, a larger mismatch standard deviation results in an average higher performance bound and produces a larger perturbation in the LB.

5. CONCLUSION

This paper considered a SISO RIS-aided localization system with RIS geometry mismatch. We proposed a closed-form solution to determine the pseudo-true parameters, which is used for MCRB derivation. The derived MCRB is validated using the empirical RMSE of a ML estimator. A phenomenon is observed whereby the bound saturates as the SNR increases.

6. REFERENCES

[1] Henk Wymeersch, Jiguang He, Benoit Denis, Antonio Clemente, and Markku Juntti, "Radio localization and mapping with reconfigurable intelligent surfaces: Challenges, opportunities, and research directions," *IEEE Veh. Technol. Mag.*, vol. 15, no. 4, pp. 52–61, 2020.

[2] Hongliang Zhang, Boya Di, Kaigui Bian, Zhu Han, H. Vincent Poor, and Lingyang Song, "Toward ubiquitous sensing and localization with reconfigurable intelligent surfaces," *Proc. IEEE*, vol. 110, no. 9, pp. 1401–1422, 2022.

[3] Rawan Alghamdi, Reem Alhadrami, Dalia Alhothali, Heba Almorad, Alice Faisal, Sara Helal, Rahaf Shalabi, Rawan Asfour, Noofa Hammad, Asmaa Shams, Nasir Saeed, Hayssam Dahrouj, Tareq Y. Al-Naffouri, and Mohamed-Slim Alouini, "Intelligent surfaces for 6G wireless networks: A survey of optimization and performance analysis techniques," *IEEE Access*, vol. 8, pp. 202795–202818, 2020.

[4] Kamran Keykhosravi, Musa Furkan Keskin, Gonzalo Seco-Granados, and Henk Wymeersch, "SISO RIS-enabled joint 3D downlink localization and synchronization," in *Proc. IEEE Int. Conf. Commun. (ICC)*, 2021.

[5] Cam Ly Nguyen, Orestis Georgiou, Gabriele Gradoni, and Marco Di Renzo, "Wireless fingerprinting localization in smart environments using reconfigurable intelligent surfaces," *IEEE Access*, vol. 9, pp. 135526–135541, 2021.

[6] Haobo Zhang, Hongliang Zhang, Boya Di, Kaigui Bian, Zhu Han, and Lingyang Song, "Metalocalization: Reconfigurable intelligent surface aided multi-user wireless indoor localization," *IEEE Trans. Wireless Commun.*, vol. 20, no. 12, pp. 7743–7757, 2021.

[7] Kamran Keykhosravi, Musa Furkan Keskin, Gonzalo Seco-Granados, Petar Popovski, and Henk Wymeersch, "RIS-enabled SISO localization under user mobility and spatial-wideband effects," *IEEE J. Sel. Top. Signal Process.*, vol. 16, no. 5, pp. 1125–1140, 2022.

[8] Boyu Teng, Xiaojun Yuan, Rui Wang, and Shi Jin, "Bayesian user localization and tracking for reconfigurable intelligent surface aided MIMO systems," *IEEE J. Sel. Top. Signal Process.*, vol. 16, no. 5, pp. 1040–1054, 2022.

[9] Hadi Sarieddeen, Mohamed-Slim Alouini, and Tareq Y. Al-Naffouri, "An overview of signal processing techniques for terahertz communications," *Proc. IEEE*, vol. 109, no. 10, pp. 1628–1665, 2021.

[10] Stefano Fortunati, Fulvio Gini, Maria S Greco, and Christ D Richmond, "Performance bounds for parameter estimation under misspecified models: Fundamental findings and applications," *IEEE Signal Process Mag.*, vol. 34, no. 6, pp. 142–157, 2017.

[11] Cüneyd Öztürk, Musa Furkan Keskin, Henk Wymeersch, and Sinan Gezici, "On the impact of hardware impairments on RIS-aided localization," in *Proc. IEEE Int. Conf. Commun. (ICC)*, 2022.

[12] Hui Chen, Ahmed Elzanaty, Reza Ghazalian, Musa Furkan Keskin, Riku Jäntti, and Henk Wymeersch, "Channel model mismatch analysis for XL-MIMO systems from a localization perspective," in *Proc. IEEE GLOBECOM*, 2022.

[13] P-A Absil, Robert Mahony, and Rodolphe Sepulchre, "Optimization algorithms on matrix manifolds," in *Optimization Algorithms on Matrix Manifolds*. Princeton University Press, 2009.

[14] Emil Björnson, Henk Wymeersch, Bho Matthiesen, Petar Popovski, Luca Sanguinetti, and Elisabeth de Carvalho, "Reconfigurable intelligent surfaces: A signal processing perspective with wireless applications," *IEEE Signal Process Mag.*, vol. 39, no. 2, pp. 135–158, 2022.

[15] Pinjun Zheng, Tarig Ballal, Hui Chen, Henk Wymeersch, and Tareq Y Al-Naffouri, "Coverage analysis of joint localization and communication in THz systems with 3D arrays," *TechRxiv preprint*, 2022, doi: 10.36227/techrxiv.21385080.v1.

[16] Arash Shahmansoori, Gabriel E. Garcia, Giuseppe Destino, Gonzalo Seco-Granados, and Henk Wymeersch, "Position and orientation estimation through millimeter-wave MIMO in 5G systems," *IEEE Trans. Wireless Commun.*, vol. 17, no. 3, pp. 1822–1835, 2018.

[17] Hui Chen, Hadi Sarieddeen, Tarig Ballal, Henk Wymeersch, Mohamed-Slim Alouini, and Tareq Y. Al-Naffouri, "A tutorial on terahertz-band localization for 6g communication systems," *IEEE Commun. Surv. Tutorials*, vol. 24, no. 3, pp. 1780–1815, 2022.

[18] Steven M Kay, *Fundamentals of statistical signal processing: estimation theory*, Prentice-Hall, Inc., 1993.

[19] Kaare Brandt Petersen, Michael Syskind Pedersen, et al., "The matrix cookbook," *Technical University of Denmark*, vol. 7, no. 15, 2008.

[20] N. Boumal, B. Mishra, P.-A. Absil, and R. Sepulchre, "Manopt, a Matlab toolbox for optimization on manifolds," *Journal of Machine Learning Research*, vol. 15, no. 42, pp. 1455–1459, 2014.